Computational and Structural Biotechnology Journal 26 (2024) 70–77

Contents lists available at ScienceDirect

Computational and Structural Biotechnology Journal

journal homepage: www.elsevier.com/locate/csbj

Research Article

Quantum theory of a potential biological magnetic field sensor: Radical pair mechanism in flavin adenine dinucleotide biradicals

Amirhosein Sotoodehfar [a,b,c], Rishabh [a,b,c], Hadi Zadeh-Haghighi [a,b,c], Christoph Simon [a,b,c,*]

[a] Department of Physics and Astronomy, University of Calgary, Calgary, AB, T2N 1N4, Canada
[b] Institute for Quantum Science and Technology, University of Calgary, Calgary, AB, T2N 1N4, Canada
[c] Hotchkiss Brain Institute, University of Calgary, Calgary, AB, T2N 1N4, Canada

ABSTRACT

Recent studies *in vitro* and *in vivo* suggest that flavin adenine dinucleotide (FAD) on its own might be able to act as a biological magnetic field sensor. Motivated by these observations, in this study, we develop a detailed quantum theoretical model for the radical pair mechanism (RPM) for the flavin adenine biradical within the FAD molecule. We use the results of existing molecular dynamics simulations to determine the time-varying distance between the radicals on FAD, which we then feed into a quantum master equation treatment of the RPM. In contrast to previous semi-classical models, which are limited to the low-field and high-field cases, our quantum model can predict the full magnetic field dependence of the transient absorption signal. Our model's predictions are consistent with experiments at physiological pH values.

1. Introduction

Magnetosensitivity is abundant throughout biology, and many biological systems are under the influence of Earth's weak magnetic field in various aspects, which range from using it as a sensory cue for migration [1–4] to the regulation of plant function and growth [5,6]. It is known that different animals, such as migratory birds [7,8], sea turtles [9,10], and some insects [11,12], sense and use Earth's magnetic field.

A number of models have been proposed to explain magnetoreception in biological systems. The most prominent among them is magnetoreception based on the radical-pair mechanism (RPM) [7,13–15] as initially proposed by Schulten et al. [16]. Spin-correlated pairs of radicals (molecules with an unpaired electron) can be created via electron transfer from one closed shell molecule to another or homolytic cleavage of a chemical bond.

Comparing the thermal energy at room temperature, 10^{-20} J, and the magnetic interaction energy, 10^{-27} J, may lead one to expect that Earth's magnetic field should have a negligible impact on biology and chemistry (or biochemistry). However, as we see in Sec. 2, the RPM model explains how Earth's weak magnetic field can change the relative yield of chemical products for certain reactions.

Thus far, the primary candidate for RPM magnetoreception is a flavoprotein molecule known as cryptochrome, in which a blue-light-activated electron transfer between the flavin adenine dinucleotide (FAD) molecule and the tryptophan triad leads to the formation of a radical pair [14,17–20].

Recently, an experimental study using electrophysiology and behavioral analyses conducted by Bradlaugh et al. challenged this cryptochrome-based RPM model for magnetoreception [21]. Their results indicate that FAD alone can also act as a biological magnetosensor.

Bradlaugh et al.'s observations suggest a possibility of a potential FAD-based RPM. The formation of radical pairs can be achieved by intramolecular electron transfer from adenine to flavin moiety in the FAD molecule under blue light excitation in aqueous solution [22]. Previously, it has been shown that the photochemistry of FAD is sensitive to external magnetic fields [22,23]. Here we investigate whether the RPM model can enable us to understand the role of the external magnetic field in FAD photochemistry. In the RPM framework, the external magnetic field alters the interconversion between singlet/triplet states. This interconversion between spin states is under the influence of several interactions, such as Zeeman, hyperfine, and exchange couplings [24].

The previous theoretical models for FAD photochemistry are based on a semi-classical approach using rate equations. These semi-classical models can only describe two extreme cases of magnetic field dependence (high field and low field) [23]. In contrast, our quantum approach provides a framework that explicitly incorporates not only the hyperfine coupling but also the Zeeman and exchange interactions, with the latter being dependent on the distance between radicals. This enables us

* Corresponding author.
E-mail addresses: amirhossein.sotoodeh@ucalgary.ca (A. Sotoodehfar), rishabh1@ucalgary.ca (Rishabh), hadi.zadehhaghighi@ucalgary.ca (H. Zadeh-Haghighi), csimo@ucalgary.ca (C. Simon).

https://doi.org/10.1016/j.csbj.2024.11.032
Received 26 July 2024; Received in revised form 20 November 2024; Accepted 20 November 2024
Available online 28 November 2024

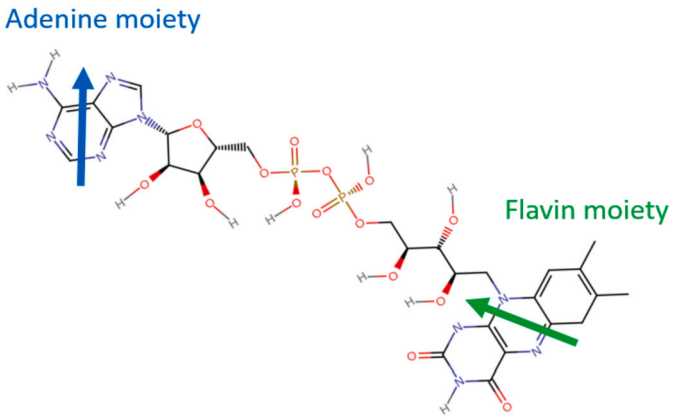

Fig. 1. Structure of flavin adenine dinucleotide. This structure is made by using the Ligand Reader and Modeler available in CHARMM-GUI [28,29]. We need to clarify that the center of the arrows (not the tips) are at the COMs of two moieties, where we assume that the radicals are located. In this illustration the arrows are meant to represent the spins.

to model the relationship between conformational dynamics and magnetic field sensitivity, leading to a description of the full magnetic field dependence.

As the exchange interaction depends on the distance between the two radicals, an understanding of the conformation of the FAD molecule is needed. The structure of FAD is shown in Fig. 1. We have used the results of existing molecular dynamics (MD) simulation in the literature on the movement of the FAD molecule in water [25]. This helps us to understand the distance between the radical spins within the molecule as a function of time. With this time-dependent distance information, we can calculate the exchange interaction and incorporate it into our quantum RPM model. For this RPM model, we used a quantum master equation, Eq. (4), to obtain the spin dynamics of the radical pair system under the influence of the above-mentioned interactions. Notice that the time-dependent behavior of exchange interaction results in a time-dependent Liouvillian for the quantum master equation. Since we are dealing with an open quantum system, we included the effect of spin relaxation and spin-selective chemical reaction of states as well.

Time-resolved transient absorption (TA) spectroscopy is a valuable technique for analyzing magnetic field effects (MFEs) [22,26]. The time profile of the transient absorption, known as $\Delta\Delta A$, represents the change in absorbance due to the magnetic field. Specifically, the double delta ($\Delta\Delta$) signifies the difference between the absorbance change without the magnetic field ($\Delta A_{B=0}$) and with the magnetic field ($\Delta A_{B=B_0}$), highlighting the magnetically induced effect on the signal [27]. As elaborated in Sec. 4, the integration of this signal over time gives the MFE. We used our quantum-based model to calculate MFE curves theoretically at physiological pH (with some reasonable simplifying assumptions regarding FAD photochemistry) as a way to validate the presented model. Our results are consistent with the experimental observations. We note that while our quantum-based model offers insights into the full magnetic field dependence within the biologically relevant pH range, it is not intended as a replacement for established semi-classical models [22,23], which are still effective in describing key aspects of the spin dynamics. Such semi-classical models, for instance, are particularly useful for capturing the pH dependence of the MFEs as well as the behavior of MFEs at low (~0 mT) and high (~20 mT) magnetic fields. In particular, modeling the full pH dependence of MFEs is not a goal of the present study.

This paper is organized as follows. The theoretical model we used to demonstrate the magnetic field effect on the spin system based on the quantum master equation is provided in Sec. 2. An overview of pre-existing molecular dynamics simulation for FAD in water solvent and how this simulation can inform us about the time-varying distance between radicals within the FAD molecule, as well as the method we used to solve the time-dependent quantum master equation, is presented in Sec. 3. In Sec. 4, we discussed the photochemistry of FAD and demonstrated a good correspondence between our theoretical model and experimental results at physiological pH.

2. Theoretical model

The biradical system within the FAD molecule consists of two radicals, A and B, one in the flavin and the other in adenine moiety, as shown in Fig. 1.

Several interactions can influence the dynamics of the spin system, such as Zeeman, hyperfine, exchange, electron dipole-dipole, spin-orbit, nuclear Zeeman, and nuclear dipole-dipole couplings. However, some of these interactions are negligible for the FAD biradical. The spin-orbit interaction, which arises from the coupling between electron spin and the magnetic field generated by the orbital motion of the electron, can be ignored for organic radicals with low symmetry and no heavy atomic nuclei [30,31]. Nuclear Zeeman coupling and dipole-dipole interaction between nuclei are also negligible compared to their electronic counterpart because the gyromagnetic ratio for nuclei is much smaller than for electrons [32]. We found that omitting the electron dipole-dipole interaction does not change the overall conclusion about the sensitivity of FAD photochemistry to the magnetic field (see Supplementary Fig. S.1 for a comparison between the magnitude of the different interactions). We introduce the four remaining couplings in the following.

The Zeeman interaction with the Hamiltonian of form

$$H_Z = -\gamma_e \vec{B}.\vec{S} \tag{1}$$

is responsible for the effect of the external magnetic field on the electronic spin system, where γ_e and $\vec{B}$ are the gyromagnetic ratio of the electron and the external magnetic field, respectively. Also, $\vec{S} = (\hat{S}_x, \hat{S}_y, \hat{S}_z)$ is the electron spin momentum. The Zeeman interaction splits the energy levels of a particle with non-zero spin (like electrons) under the influence of an external magnetic field. In our modeling, we assumed that the direction of the external magnetic field is aligned with the z-axis of the coordinate system.

The hyperfine interaction takes care of the coupling between atomic nuclei and the spin of an electron. Fundamentally speaking, hyperfine coupling is composed of two interactions. The first is because of the dipole-dipole coupling between the magnetic moments of the electron and the nucleus, analogous to the classical dipolar coupling of two magnetic moments. The other is the Fermi contact term, which is due to the non-zero probability density of the electron at the nucleus. Fermi contact is an isotropic interaction and happens in radicals with p, d, or f orbitals [33]. The hyperfine coupling has the following form:

$$H_{HF} = \gamma_e \vec{S} \cdot \vec{\vec{A}} \cdot \vec{I}. \tag{2}$$

The hyperfine tensor $\vec{\vec{A}}$ can be calculated using density functional theory (DFT). Because of rotational averaging due to molecular motion in a solution, we only consider the isotropic hyperfine interaction.

We assumed an effective hyperfine interaction with one spin-1/2 nucleus for each radical, one for the flavin moiety and the other for the adenine moiety. For the hyperfine coupling constants (HFCCs) of each radical, we first calculated the effective HFCCs, which are approximations representing the average contribution of all nuclei (see Eq. (5)), using the results of the existing *ab initio* calculations [34,35], yielding values of $a_{ade} = 1.37$ mT and $a_{fla} = 1.07$ mT. We then optimized these values manually (jointly with relaxation and reaction rates), testing multiple combinations close to the above values, and found that the HFCC values $a_{ade} = 1.55$ mT, $a_{fla} = 1.3$ mT provided the best agreement with experimental TA signals (see Supplementary Figs. S.2 and S.3). Given the interaction between the electronic and nuclear spins via hyperfine coupling, the required Hilbert space can be defined as $S_A \otimes I_A \otimes S_B \otimes I_B$, where S_A and S_B represent the electronic spin on each radical, and similarly, I_A and I_B represent the nuclear spins.

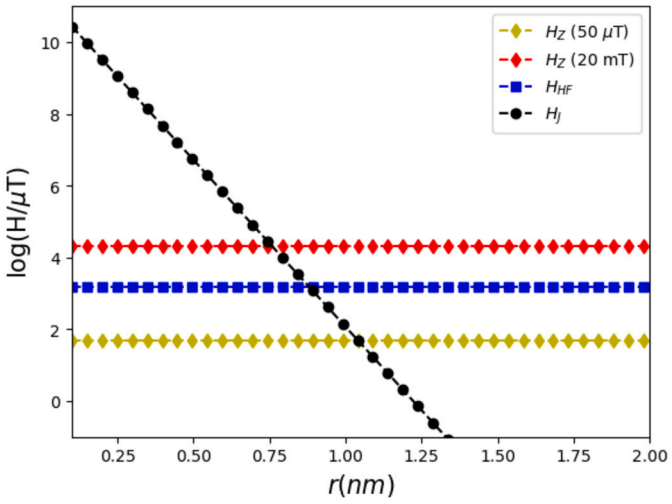

Fig. 2. Logarithmic plot of the magnitudes of the Zeeman (H_Z), hyperfine (H_{HF}), and exchange (H_J) interactions. Two different magnitudes of the magnetic field, 50 μT (geomagnetic field) and 20 mT, are illustrated. The HFCC is 2 mT.

The coupling between two unpaired electrons due to the overlap of their spatial wave function is called the exchange interaction:

$$H_J = -J_0 e^{-\beta r}(\vec{S}_A \cdot \vec{S}_B - \hat{1}), \tag{3}$$

where for the biradical of FAD, $J_0 = 2.3 \times 10^8$ mT, $\beta = 21.4$ nm^{-1} [36]. Notice that this coupling is very large for short distances, but drops rapidly with distance. The exchange interaction stems from the exchange symmetry of electrons (indistinguishable particles and fermions) and the Coulomb force in between them.

As the exchange interaction is dependent on the distance between two radicals, it is important to be aware of the conformation of the molecule over time and the relative position of the flavin and the adenine moieties. Fig. 2 illustrates a comparison between these three above-mentioned interactions for different distances.

As evident, the exchange interaction is dominant at small distances, and therefore, the effect of the Zeeman coupling is negligible. However, by gradually increasing the distance, the energy related to the exchange interaction becomes negligible, and the magnetic field effect can be retrieved.

Now that we understand the internal interactions of the spin system, we can model this open quantum system using the quantum master equation approach to formulate the evolution of the density matrix of the spin states, $\hat{\rho}(t)$, in time. The density operator fully describes the system dynamics and demonstrates both the probabilities of each state (diagonal elements of the density matrix operator) as well as coherences (off-diagonal elements of the density matrix operator). However, as we discuss in Sec. 4, the coherences are negligible in our case.

Investigating the dynamics of this open quantum system can be done using the stochastic Liouville master equation [30]:

$$\frac{d}{dt}\hat{\rho}(t) = -\hat{\hat{\mathcal{L}}}(t)[\hat{\rho}(t)], \tag{4}$$

where for the Liouvillian we have

$$\hat{\hat{\mathcal{L}}} = j\hat{\hat{\mathcal{H}}} + \hat{\hat{\mathcal{K}}} + \hat{\hat{\mathcal{R}}},$$

where j is the imaginary unit $\sqrt{-1}$, and $\hat{\hat{\mathcal{H}}}, \hat{\hat{\mathcal{K}}}$, and $\hat{\hat{\mathcal{R}}}$ are the commutator superoperator corresponding to the Hamiltonian, chemical reactions, and spin relaxation, respectively. The Hamiltonian includes the three interactions we have discussed above

$$\hat{H} = \hat{H}_Z + \hat{H}_{HF} + \hat{H}_J,$$

and for the Hamiltonian superoperator we have

$$\hat{\hat{\mathcal{H}}} = \hat{H} \otimes \hat{1} - \hat{1} \otimes \hat{H}.$$

The spin states of a radical pair can undergo different chemical reactions, and we use the Haberkorn model for spin-selective first-order reactions [30] with the following superoperator:

$$\hat{\hat{\mathcal{K}}} = \frac{k_s}{2}(\hat{P}^S \otimes \hat{1} + \hat{1} \otimes \hat{P}^S) + \frac{k_t}{2}(\hat{P}^T \otimes \hat{1} + \hat{1} \otimes \hat{P}^T),$$

where k_s and k_t are the singlet and triplet reaction rates, respectively. Further, $\hat{P}^S$ and $\hat{P}^T$ are the singlet and triplet projection operators, respectively. The singlet and triplet states are defined as:

$$|S\rangle = \frac{1}{\sqrt{2}}\left(|\uparrow_A\downarrow_B\rangle - |\downarrow_A\uparrow_B\rangle\right)$$
$$|T_+\rangle = |\uparrow_A\uparrow_B\rangle$$
$$|T_0\rangle = \frac{1}{\sqrt{2}}\left(|\uparrow_A\downarrow_B\rangle + |\downarrow_A\uparrow_B\rangle\right)$$
$$|T_-\rangle = |\downarrow_A\downarrow_B\rangle.$$

Moreover, the relaxation superoperator [30]

$$\hat{\hat{\mathcal{R}}} = k_r^A\left(\frac{3}{4}\hat{1} \otimes \hat{1} - \hat{S}_{A,x} \otimes \hat{S}^T_{A,x} - \hat{S}_{A,y} \otimes \hat{S}^T_{A,y} - \hat{S}_{A,z} \otimes \hat{S}^T_{A,z}\right)$$
$$+ k_r^B\left(\frac{3}{4}\hat{1} \otimes \hat{1} - \hat{S}_{B,x} \otimes \hat{S}^T_{B,x} - \hat{S}_{B,y} \otimes \hat{S}^T_{B,y} - \hat{S}_{B,z} \otimes \hat{S}^T_{B,z}\right),$$

takes care of the relaxation process of the elements of the spin density matrix $\hat{\rho}(t)$. The relaxation superoperator introduced here accounts for random time-dependent local fields and spin rotation.

To set the rate values in our calculations, we initially used rate coefficients related to physiological pH from [22]. Based on these coefficients, as explained earlier in this section, we explored various sets of rate values (jointly with HFCCs), ultimately selecting those that yielded the best agreement with experimental results (see Supplementary Figs. S.2 and S.3), resulting in values of 9×10^5 s^{-1} and 7×10^5 s^{-1} for relaxation and chemical reaction rates, respectively.

For a system with a time-independent Hamiltonian, the Liouvillian is constant over time, and hence, the solution to Eq. (4) is given by the following expression

$$\hat{\rho}(t) = e^{-\hat{\hat{\mathcal{L}}}t}[\hat{\rho}(0)],$$

where $\hat{\rho}(0)$ is the initial state.

The fractional singlet yield produced by the RPM can be calculated as follows [30]

$$\Phi^S = k_s \int_0^\infty \mathrm{Tr}\left[\hat{P}^S\hat{\rho}(t)\right]dt.$$

Analyzing the effect of the distance between the two radicals on the singlet yield of this spin system is a key step in our calculations. The singlet yield of the system is illustrated in Fig. 3 as a function of the applied magnetic field for various values of r.

As evident, the profile of the singlet yield varies with the distance between the radicals due to the dependence of the exchange interaction on this distance. At short distances (< 0.7 nm), the magnitude of the exchange coupling is much greater than the Zeeman interaction, and therefore, no MFE can be seen (no dependency of $\Phi^{S(S)}$ on changing the magnetic field). At larger distances (> 1.5 nm), we only see the effect of Zeeman and hyperfine interactions. A mesh-grid style graph of $\Phi^{S(S)}$ for different distances and magnetic fields is provided in Supplementary Fig. S.5.

3. FAD conformations and time-dependent quantum systems

The fluorescence properties of FAD show that this molecule exists in both closed and open conformations [37], as depicted in Fig. 4. The closed conformation refers to the case in which the adenine and flavin moieties stack on each other, and on the other hand, in the open conformation, the distance between these two moieties is larger than the former case [38].

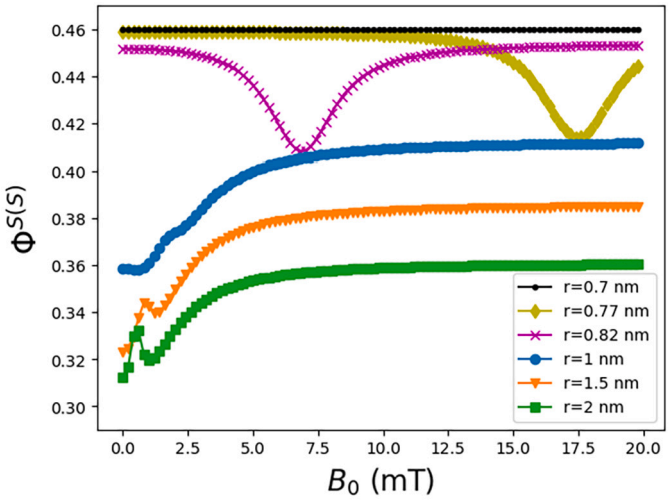

Fig. 3. Singlet yield of a radical pair system as a function of the magnetic field with the initial singlet state, $\Phi^{S(S)}$, for different distances between the radicals. The relaxation (k_r^A, k_r^B) and chemical reaction rates (k_s, k_t) are 9×10^5 s^{-1} and 7×10^5 s^{-1}, respectively. The plot corresponding to $r = 0.7$ nm is flat and equal to 0.46.

Experimental evidence based on studying the fluorescence quenching of FAD shows that in the pH range from 4 to 9, this molecule is observed around 80% of the time in its closed conformation [41,42]. Radoszkowicz et al. have studied the conformation space of FAD in water using MD simulation [25]. In their study, they performed MD simulation to obtain the distance between the centers of mass (COM) of the adenine and isoalloxazine ring structures while FAD is located in a water solvent. They have suggested $r = 0.6$ nm as a cutoff distance to discriminate between the open and stacked conformation. Their result for the distance between the two COMs is illustrated in Fig. 5, with a simulation time of 650 ns.

In our model, we have chosen the COMs of the adenine and flavin moieties as proxies for the unpaired electrons in the molecular orbitals of FAD. Having the results of the MD simulation for the distance between the radicals, we then need to feed them into the quantum master equation. To solve the quantum master equation with time-dependent Liouvillian, we assumed that the Liouvillian is constant during very small time steps, and calculated its evolution in time by solving the following recurring equation:

$$\hat{\rho}_{i+1} = e^{-\hat{\hat{\mathcal{L}}}_i \Delta t} \hat{\rho}_i,$$

where Δt is the time steps, $\hat{\rho}_{i+1}$ is the density operator at time $(i+1)\Delta t$, and $\hat{\hat{\mathcal{L}}}_i$ and $\hat{\rho}_i$ are the Liouvillian and density operator at time $i\Delta t$, respectively. Notice that $\hat{\rho}_0 = \hat{\rho}(0)$. In our study, all calculations related to solving the master equation were performed using the Python programming language.

In order to avoid the extreme computational cost in solving the master equation for many different distances, we averaged the distance over time windows of length 1 ns. The averaged version of the original results shown in Fig. 5, which has been fed into the quantum master equation, is provided in Supplementary Fig. S.6. We calculated $\hat{\rho}_{i+1}$ for each time step of length $\Delta t = 1$ ns using Python. For this purpose, we used an iterative algorithm. We first constructed the matrices for the Hamiltonian, chemical reaction, and spin relaxation superoperators at some given time step $i\Delta t$, and used them to calculate the corresponding matrix for the Liouvillian superoperator also at $t = i\Delta t$. Using this Liouvillian superoperator matrix, we computed the matrix corresponding to $e^{-\hat{\hat{\mathcal{L}}}_i \Delta t}$ and multiplied it with the $\hat{\rho}_i$ matrix to get the density matrix at the next time step, i.e., $\hat{\rho}_{i+1}$. We then repeated this process for the required number of times.

4. Magnetic field effects on the transient absorption

In this section, we make a connection between our quantum theoretical model and existing experimental observations. For this purpose, a brief understanding of the FAD photochemistry is required. Under blue light excitation of the flavin moiety and an intramolecular electron transfer from the adenine moiety, a biradical can be formed. This biradical undergoes spin-selective chemical reaction, resulting in magnetic

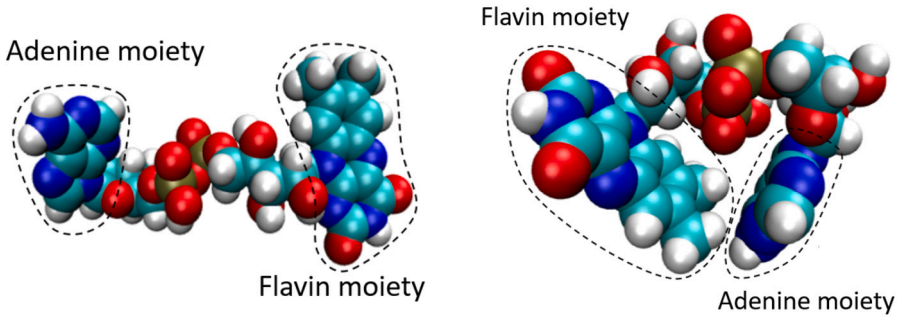

Fig. 4. FAD molecule depicted in the open (left) and closed (right) configurations. The configurations are generated by GROMACS [39] and depicted by VMD computer program [40].

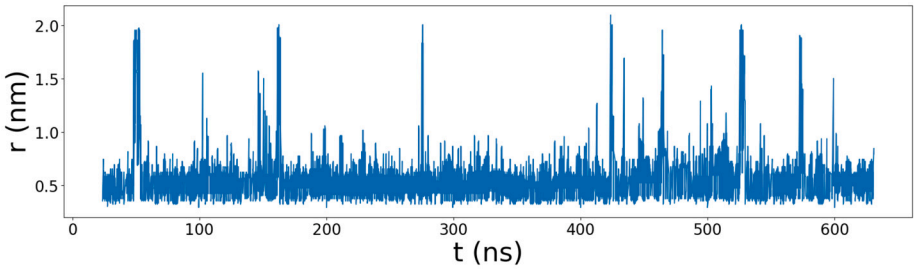

Fig. 5. Distance between the COMs of the adenine and isoalloxazine ring structures of FAD. These data points are extracted from Fig. 2 (top plot) of [25] using an online plot digitized tool.

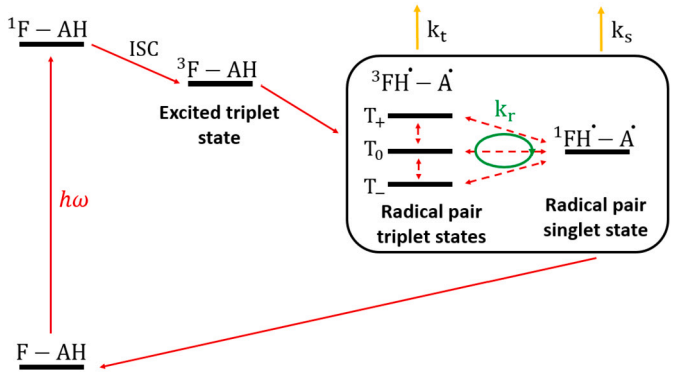

Fig. 6. Reaction scheme for photochemistry of FAD. k_s and k_t denote the reaction rates for the singlet and triplet states, respectively. The relaxation rate, k_r, is equal for both the singlet and triplet states.

field effects on the photochemistry of FAD [22]. The scheme showing the FAD photochemistry is provided in Fig. 6.

Several chemical kinetic models have been proposed to explain the magnetic field effects on the photochemistry of FAD at different pH values [23,26]. While these models are well suited for describing the pH dependence of the magnetic field effects, as discussed above, they do not involve a full quantum mechanical treatment of the radical pair dynamics, including the Zeeman and exchange interactions. This restricts their predictive power to the two extreme cases of low and high magnetic fields.

In the quantum approach, the state of the radical pair is described by the density matrix. The density matrix in the basis of singlet-triplet states (S, T_+, T_0, and T_-) can be described as follows:

$$\hat{\rho}(t)=\begin{pmatrix}\rho_{SS} & \rho_{T_+S} & \rho_{T_0S} & \rho_{T_-S}\\ \rho_{ST_+} & \rho_{T_+T_+} & \rho_{T_0T_+} & \rho_{T_-T_+}\\ \rho_{ST_0} & \rho_{T_+T_0} & \rho_{T_0T_0} & \rho_{T_-T_0}\\ \rho_{ST_-} & \rho_{T_+T_-} & \rho_{T_0T_-} & \rho_{T_-T_-}\end{pmatrix}(t).$$

The diagonal and off-diagonal elements of the density matrix show the concentration of each state and the coherence, respectively. As shown in an earlier section, the time evolution (Eq. (4)) of the density matrix is governed by the master equation. This approach allows a systematic treatment for all magnetic field values and can also incorporate the effects of varying distances between the radicals.

On the other hand, in the semi-classical approach, the state of the radical pair is described by a population vector, whose time evolution is governed by a rate equation. Rate equations are a set of equations relating the rate of change of an individual state population (its first derivative in time) to a linear combination of the populations of all states. The semi-classical approach only involves the diagonal elements of the density matrix in the S-T basis (the populations) and neglects the coherences. We found that neglecting the coherences turns out to be a fair assumption for this radical pair system as they die out very quickly (see Supplementary Fig. S.7). The form of the rate equations for this model is given as follows.

$$\frac{d}{dt}\begin{pmatrix}[S]\\ [T_+]\\ [T_0]\\ [T_-]\end{pmatrix}=\begin{pmatrix}k_{SS} & \cdots & k_{ST_-}\\ \vdots & \ddots & \vdots\\ k_{T_-S} & \cdots & k_{T_-T_-}\end{pmatrix}\begin{pmatrix}[S]\\ [T_+]\\ [T_0]\\ [T_-]\end{pmatrix},$$

where $[S],[T_+],[T_0]$, and $[T_-]$ are the populations of different states, and k_{ij} are the rates for transition between states. Notice that the magnitude of different interactions defines these rates. As discussed in [23], in the absence of a magnetic field ($B=0$), only the hyperfine coupling with the rate of k_{hfc} is responsible for the interconversion between these four states. k_{hfc} depends on the effective local magnetic field of each nucleus and has the following expression:

$$k_{hfc}=\frac{2(B_1^2+B_2^2)}{\hbar(B_1+B_2)}.$$

In order to calculate B_1 and B_2, we use:

$$B_i(i=1,2)=\left(\sum_k\left(I_{ik}(I_{ik}+1)a_{ik}^2\right)\right)^{\frac{1}{2}}, \tag{5}$$

where a_{ik} and I_{ik} represent the HFCC and the nuclear spin quantum number of the k-th nucleus in the ith radical, respectively. On the other hand, in the presence of a large magnetic field, the energy levels of the T_+ and T_- states are separated from the S and T_0 states due to the Zeeman energy. As explained in [23], this implies that the electron spin relaxation rate (k_r) governs the interconversion between T_+ and T_- states and S, T_0 states, and k_{hfc} is responsible for the interconversion between S and T_0 states.

As it is evident, this model fails to predict the behavior of the system for an intermediate magnetic field, where hyperfine and Zeeman interactions are not negligible to each other. Moreover, this model does not include the effects of the distance-dependent exchange interaction and thus cannot capture the impact of the conformational dynamics on the magnetic field effects.

As a comparison between quantum master equation and semi-classical rate equation approaches, let us look at the population of singlet and triplet states for these two models under the same conditions. The results are illustrated in Fig. 7.

In Fig. 7, notice that in the middle plot ($r=0.5$ nm), no interconversion between singlet and triplet states can be observed, resulting in no magnetic field effect. This is due to the strong exchange interaction at small distances. As we discussed in Sec. 2, in order to address the effect of the limited number of hyperfine interactions in our quantum model, we implemented an effective HFCC approach. Note that a full multi-nuclei description might reduce the observed oscillations in the quantum model.

Previously, semi-classical models have mainly been used to explain the changes in the TA signal in the presence and absence of a magnetic field. The idea behind TA spectra is to first excite the sample with a pump pulse and then, after a period of time, send a probe pulse to obtain the absorption spectra of the excited sample.

The time profile of MFE is calculated by subtracting TA signals for zero and high ($B=B_0$) magnetic fields:

$$\Delta\Delta A_{(B=B_0,t)}=\Delta A_{(B=B_0,t)}-\Delta A_{(B=0,t)}. \tag{6}$$

As treated by Murakami et al. [23], the time-resolved MFE action signal is given by $\Delta\Delta A(t)=\epsilon_R\Delta C_R(t)+\epsilon_T\Delta C_T(t)$, where ΔC_R and ΔC_T represent the contributions of the radical pair triplet state and the excited triplet state (see Fig. 6) on the MFE action spectra, respectively. ϵ_R and ϵ_T are the template spectra for their corresponding states.

However, the photochemistry model proposed by Murakami et al. [23] is valid for low pH values. In their model, there is electron transfer/back electron transfer between the excited triplet state and the radical pair triplet state. At higher pH values, there is only the feeding term from the excited triplet state to the radical pair triplet state (The feeding term from the radical pair triplet state to the excited triplet states decays as the concentration of protons, $[H^+]$, increases) [22]. Under this condition, starting from the radical pair triplet state works well for analyzing the dynamics of the system. Thus, for simplicity, we only take into account the contribution of the radical pair triplet state while calculating $\Delta\Delta A$, i.e., we assumed $\Delta C_T=0$. Implementing the population of the triplet state, up to a scaling factor, into Eq. (6) [23] results in:

$$\Delta\Delta A=\mathrm{fac}\left(\left([T_+]+[T_0]+[T_-]\right)_{B=B_0}-\left([T_+]+[T_0]+[T_-]\right)_{B=0}\right).$$

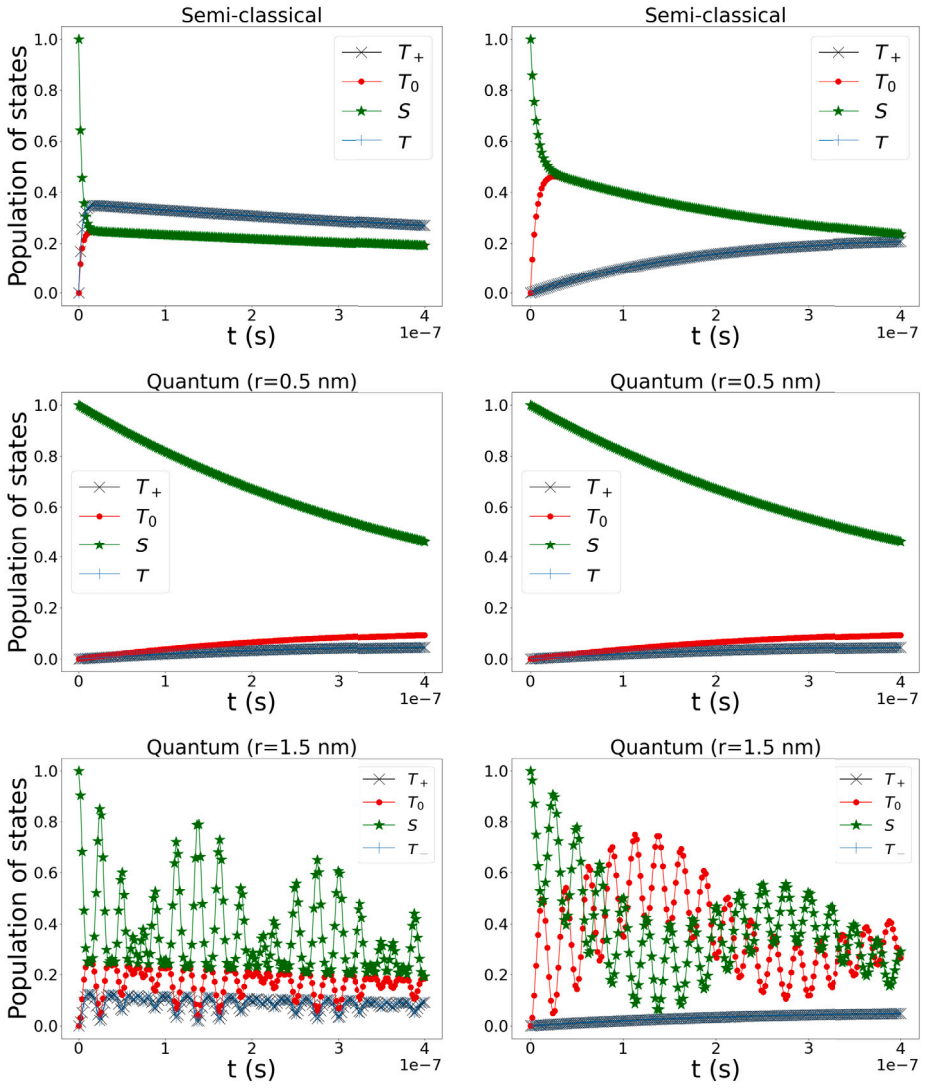

Fig. 7. Time evolution of the singlet (S) and triplet (T_+, T_0, and T_-) states for two different cases: (a) B = 0 (low magnetic field) and (b) B = 20 mT (high magnetic field). The initial state is the singlet state. Relaxation (k_r^A, k_r^B) and reaction rates (k_s, k_t) are $7\times10^5 s^{-1}$ and 9×10^5 s^{-1}, respectively.

Notice that in the quantum model, the concentrations are defined as $[T_i] = \rho_{ii}$. The calculated $\Delta A_{(B=20\text{ mT},t)}$ signal obtained from the quantum master equation is illustrated in Fig. 8. See Supplementary Fig. S.4 for a comparison between theoretical and experimental $\Delta\Delta A$ signals. Although our calculation contains several assumptions, our theoretical curve is in quantitative agreement with the experimental plot. The experimental curve corresponds to averaging over many individual FAD molecules.

Another related quantity that is used to show that the photochemistry of FAD is sensitive to magnetic fields is the MARY (Magnetically Affected Reaction Yield) curves [22,43]. The MARY curve can be obtained by dividing $\Delta\Delta A_{(B=B_0,t)}$ by $\Delta A_{(B=0,t)}$ and integrating over the whole time window [22].

$$\text{MFE}\% = \int_0^\infty \frac{\Delta\Delta A_{(B=B_0,t)}}{\Delta A_{(B=0,t)}} dt \times 100\%. \tag{7}$$

The calculated MARY curve at physiological pH is shown in Fig. 9 in comparison with the experimental MFE. A quantitative agreement can be observed between our calculated MFE and experimental results on MFE curves obtained by Antill et al. [22]. This verifies that the proposed RPM model is able to explain the magnetic field sensitivity of FAD photochemistry.

5. Discussion

In the present work, we investigated the MFEs on the spin dynamics of a biradical formed within molecule FAD, which may be a possible biological magnetic field sensor. We used the RPM model to evaluate how the magnetic field changes the spin dynamics and photochemistry of FAD.

The populations of singlet and triplet states are obtained by solving the Lindblad quantum master equation for a biradical formed in the FAD molecule. Our quantum master equation includes Zeeman, hyperfine, and exchange interactions. Other interactions, such as electron dipole-dipole, spin-orbit, nuclear Zeeman, and nuclear dipole-dipole interactions, are ignored because of their weak effect on our system. The openness of this system is modeled via relaxation and chemical reaction processes.

The exchange interaction is dependent on the distance between two radicals, and altering this distance results in a different MFE. To study the effects of the conformational dynamics of FAD, we used the results of MD simulations of a molecule in an aqueous solution, which are

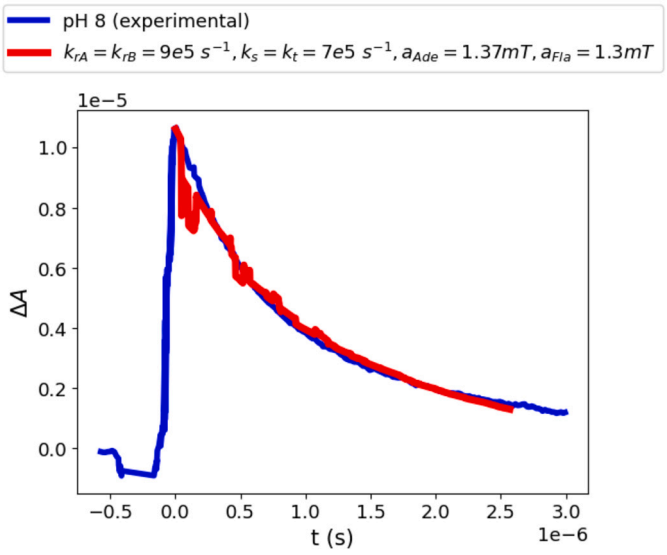

Fig. 8. Time profile of the transient absorption $\Delta A_{(B=20\ \mathrm{mT},t)}$. For the calculated signal, the relaxation rates (k_r^A, k_r^B) and the chemical reaction rates (k_s, k_t) are 9×10^5 and $7\times10^5\ s^{-1}$, respectively. The experimental ΔA time profile (pH = 8) is extracted manually from [22]. The experimental signal represents an averaging over a large number of FAD molecules. The Magnetic field is 20 mT for both signals.

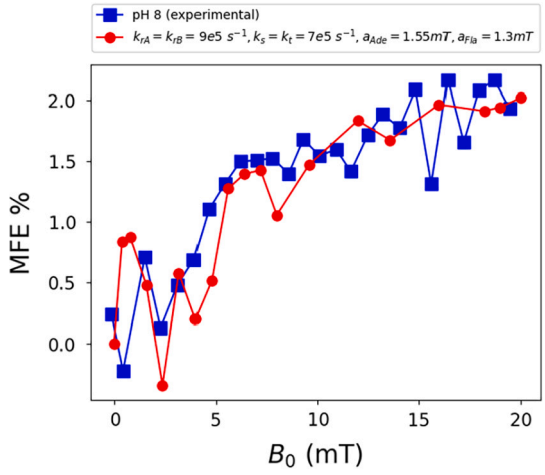

Fig. 9. Calculated and experimental magnetic field effects (MFEs) of FAD at physiological pH values. This plot shows the magnetically affected reaction yield (MARY) spectra as defined in Eq. (7). The experimental data points are extracted manually from Fig. 3(a) in [22].

consistent with fluorescence quenching of FAD [25], to obtain its configuration in time. Fig. 3 illustrates changes in singlet quantum yield for different distances and magnetic fields. MFE can be observed only for relatively open conformations of the molecule. Our theoretical model predicts that the lifetime in the open conformation is enough to observe non-zero MFE.

Our quantum-based model, which is powered by the MD simulation results, has several advantages over previous semi-classical models. The semi-classical models formulate the spin dynamics of the biradical within FAD via rate equations and do not include the effects of the Zeeman interaction at intermediate fields and the exchange interactio. Because of this, these models are limited to only low and high magnetic field cases and cannot describe the full magnetic field dependence or the effects of the conformational dynamics. In our approach, the quantum aspect primarily comes from using a Hamiltonian that includes quantum interactions. It is worth noting that we found the coherences in the density matrix to be negligible.

As a method to verify our model and compare it to experimental observations, we calculated the TA signal, as shown in Fig. 8 and Fig. 9, and compared it with experimental results from TA spectroscopy. It is worth keeping in mind that our theoretical calculation of this signal contains some assumptions such as ignoring the role of the excited triplet state, as discussed in previous sections. With some fitting of parameters in a reasonable range, the comparison shows good quantitative agreement between our theoretical model and experimental results.

As a suggestion for future research on this topic, there is room for performing accurate MD simulations for different conditions. First, the MD simulation taken from [25] is for the oxidized form of FAD. In future work, one can extend our model by incorporating the radicalized form of FAD into the MD simulation to better capture other key interactions, such as the Coulomb attraction in the radical ion pair. Different pH values change the protonation state of the molecule, leading to different conformations for the dynamics of FAD in water. These changes result in a different time profile for the distance between COMs, and subsequently lead to different magnetic field effects. Different protonation states require different parameters, and these new parameters can be obtained by a process known as parametrization, which requires *ab initio* calculations.

Future studies could explore how the finite lifetime of the open conformation of FAD may influence singlet-triplet oscillations and its potential role in enhancing magnetoreception. To further explore the pH dependence of the MFEs, one can use more complex kinetic equations for different pH values, as has been done in previous semi-classical models [22,23], and use the present open quantum system model to calculate the magnetic field dependencies. Note that the biradical creation within the FAD molecule can be studied using *ab initio* methods. Although the reduction of isoalloxazine to semiquinone is known, *ab initio* calculations can give us a better understanding of how adenine becomes a radical and of the placement of the radicals within the molecule for a more accurate estimate of the distance between the radicals.

As discussed in Sec. 2, adding more hyperfine couplings to the system increases the computational cost exponentially. There are existing semi-classical ways to overcome this problem, such as Shushin's two-site model [44] and a work done by Lewis et al. [45]. As a possible future work, one can implement these models for the hyperfine coupling into our present open-system model and make it more realistic and powerful. On the experimental side, more *in vivo* and *in vitro* experiments are required, for example, on magnetic field dependence, to understand the role of FAD biradicals in magnetosensitivity in various organisms. Given our quantum-theoretical model for FAD biradicals, a better insight into such experiments will be available. Also, this quantum model based on the RPM can be applied to other studies about the MFEs on the circadian clock, neurogenesis, and stem cell growth. [46–48].

CRediT authorship contribution statement

Amirhosein Sotoodehfar: Investigation, Formal analysis, Visualization, Writing – original draft. **Rishabh:** Writing – review & editing, Methodology. **Hadi Zadeh-Haghighi:** Writing – review & editing, Supervision, Methodology, Conceptualization. **Christoph Simon:** Writing – review & editing, Supervision, Methodology, Funding acquisition, Conceptualization.

Declaration of competing interest

The authors declare that the research was conducted in the absence of any commercial or financial relationships that could be construed as a potential conflict of interest.

Acknowledgements

This work was supported by the Natural Sciences and Engineering Research Council of Canada through its Discovery Grant Program and

the Alliance Quantum Consortia Grant 'Quantum Enhanced Sensing and Imaging (QuEnSI)'. The authors would like to thank Dennis Salahub, Belinda Heyne, Peter Tieleman, Hristina Zhekova, Valentina Corradi, DB Sridhar, and Rishabh Shukla for their valuable input.

Appendix A. Supplementary material

Supplementary material related to this article can be found online at https://doi.org/10.1016/j.csbj.2024.11.032.

References

[1] Johnsen S, Lohmann KJ. The physics and neurobiology of magnetoreception. Nat Rev Neurosci 2005;6:703–12. https://doi.org/c2cd9t.
[2] Mouritsen H. Chapter 15 - Magnetoreception in birds and its use for long-distance migration. In: Sturkie's avian physiology; 2022. p. 233–56. https://doi.org/nkrr.
[3] Zadeh-Haghighi H, Simon C. Magnetic field effects in biology from the perspective of the radical pair mechanism. J R Soc Interface 2022;19:193. https://doi.org/nkrs.
[4] Aiello C, Lodesani A, Gabalski A, Andres G, Payne O. The tadpole experiment. Website; 2024.
[5] Maffei ME. Magnetic field effects on plant growth, development, and evolution. Front Plant Sci 2014;5:445. https://doi.org/gjc5w3.
[6] Radhakrishnan R. Magnetic field regulates plant functions, growth and enhances tolerance against environmental stresses. Physiol Mol Biol Plants 2019;25:1107–19. https://doi.org/gmkjzx.
[7] Wiltschko W, Wiltschko R. Magnetic orientation and magnetoreception in birds and other animals. J Comp Physiol A 2005;19:675–93. https://doi.org/ftpgkj.
[8] Cochran WW, Mouritsen H, Wikelski M. Migrating songbirds recalibrate their magnetic compass daily from twilight cues. Science 2004;304:405–8. https://doi.org/dpb55b.
[9] Lohmann KJ, Cain SD, Dodge SA, Lohmann CM. Regional magnetic fields as navigational markers for sea turtles. Science 2001;294:364–6. https://doi.org/bspfcj.
[10] Lohmann KJ, Putman NF, Lohmann CM. The magnetic map of hatchling loggerhead sea turtles. Curr Opin Neurobiol 2012;22:336–42. https://doi.org/bfw656.
[11] reppert SM, Gegear RJ, Merlin C. Navigational mechanism of migrating monarch butterflies. Trends Neurosci 2010;33:399–406. https://doi.org/bfknmw.
[12] Mouritsen H. Long-distance navigation and magnetoreception in migratory animals. Nature 2018;558:50–9. https://doi.org/gdq2rp.
[13] Clites BL, Pierce JT. Identifying cellular and molecular mechanisms for magnetosensation. Annu Rev Neurosci 2017;4:231–50. https://doi.org/gdz6pk.
[14] Hore PJ, Mouritsen H. The radical-pair mechanism of magnetoreception. Annu Rev Biophys 2016;45:299–344. https://doi.org/gf247v.
[15] Adams B, Sinayskiy I, Petruccione F. An open quantum system approach to the radical pair mechanism. Sci Rep 2018;8:15719. https://doi.org/gfjp3f.
[16] Schulten K, Swenberg CE, Weller A. A biomagnetic sensory mechanism based on magnetic field modulated coherent electron spin motion. Z Phys Chem 1978;111:1–5. https://doi.org/dmg43r.
[17] Kavet R, Brain J. Cryptochrome in mammals and birds: clock or magnetic compass. Physiology 2021;36:183–94. https://doi.org/nkrt.
[18] Ritz T, Adem S, Schulten K. A model for photoreceptor-based magnetoreception in birds. Biophys J 2000;78:707–18. https://doi.org/fct279.
[19] Xu J, Jarocha LE, Zollitsch T, et al. Magnetic sensitivity of cryptochrome 4 from a migratory songbird. Nature 2021;594:535–40. https://doi.org/gkdk.
[20] Kattnig DR, Hore PJ. The sensitivity of a radical pair compass magnetoreceptor can be significantly amplified by radical scavenger. Sci Rep 2017;7:11640. https://doi.org/gbx9gf.
[21] Bradlaugh AA, Fedele G, Munro AL, et al. Essential elements of radical pair magnetosensitivity in Drosophila. Nature 2023;615:111–6. https://doi.org/grtjfx.
[22] Antill LM, Woodward JR. Flavin adenine dinucleotide photochemistry is magnetic field sensitive at physiological pH. J Phys Chem Lett 2018;9:2691–6. https://doi.org/kwsh.
[23] Murakami M, Maeda K, Arai T. Dynamics of intramolecular electron transfer reaction of FAD studied by magnetic field effects on transient absorption spectra. J Phys Chem A 2005;109:5793–800. https://doi.org/c3xmfm.
[24] Babcock NS, Kattnig DR. Electro-electron dipolar interaction poses a challenge to the radical pair mechanism of magnetoreception. J Phys Chem Lett 2020;11:2414–21. https://doi.org/g4n4dq.
[25] Radoszkowicz L, Huppert D, Nachliel E, Gutman M. Sampling the conformation space of FAD in water-methanol mixtures through molecular dynamics and fluorescence measurements. J Phys Chem A 2010;114:1017–22. https://doi.org/dkrzdz.
[26] Stob S, Kemmink J, Kaptein R. Intramolecular electron transfer in flavin adenine dinucleotide. Photochemically induced dynamic nuclear polarization study at high and low magnetic fields. J Phys Chem Soc 1989;111:7036–42. https://doi.org/b45w48.
[27] Horiuchi M, Maeda K, Arai T. Magnetic field effect on electron transfer reactions of flavin derivatives associated with micelles. Appl Magn Reson 2003;23:309–18. https://doi.org/fpn2h9.
[28] Jo S, Kim T, Iyer VG, Im W. CHARMM-GUI: a web-based graphical user interface for CHARMM. J Comput Chem 2008;29:1859–65. https://doi.org/d6b66x.
[29] Kim S, Lee J, Jo S, Brooks III CL, Lee HS, Im W. CHARMM-GUI ligand reader and modeler for CHARMM force field generation of small molecules. J Comput Chem 2017;38:1879–86. https://doi.org/gbk7dr.
[30] Player TC. Spin dynamics calculations applied to systems of potential biological significance. PhD thesis. University of Oxford; 2021.
[31] Khudyakov IV, Serebrennikov YA, Turro NJ. Spin-orbit coupling in free-radical reactions: on the way to heavy elements. Chem Rev 1993;93:537–70. https://doi.org/dj3532.
[32] Schweiger A, Gunnar J. Principles of pulse electron paramagnetic resonance; 2001.
[33] Alvarez PH. Simulation of avian magnetoreception in quantum computers. M.Sc. thesis. Universidade Estadual de Campinas; 2023.
[34] Lee AA, Lua JC, Hogben HJ, Biskup T, Kattnig DR, Hore P. Alternative radical pairs for cryptochrome based magnetoreception. J R Soc Interface 2014;11. https://doi.org/nkrq.
[35] Wetmore SD, Boyd RJ, Eriksson LA. Theoretical investigation of adenine radicals generated in irradiated DNA components. J Phys Chem B 1998;102:10602–14. https://doi.org/bjfwhq.
[36] Zhukov IV, et al. Exchange interaction in short-lived flavine adenine dinucleotide biradical in aqueous solution revisited by CIDNP (chemically induced dynamic nuclear polarization) and nuclear magnetic relaxation dispersion. Magn Reson 2021;2:139–48. https://doi.org/nkrv.
[37] Islam MS, Honma M, Nakabayashi T, Kinjo M, Ohta N. pH dependence of the fluorescence lifetime of FAD in solution and in cells. Int J Mol Sci 2013;14:1952–63. https://doi.org/gchngt.
[38] Chosrowjan H, Taniguchi S, Mataga N, Tanaka F, Visser AJWG. The stacked flavin adenine dinucleotide conformation in water is fluorescent on picosecond timescale. Chem Phys Lett 2003;378:354–8. https://doi.org/c9dtv2.
[39] Berendsen HJC, van der Spoel D, van Drunen R. GROMACS: a message-passing parallel molecular dynamics implementation. Comput Phys Commun 1995;91:43–56. https://doi.org/ckwz3n.
[40] Humphrey W, Dalke A, Schulten K. VMD: visual molecular dynamics. J Mol Graph 1996;14:27–8. https://doi.org/b3tgfk.
[41] Galbán J, Sanz-Vicente I, Navarro J, de Marcos S. The intrinsic fluorescence of FAD and its application in analytical chemistry: a review. Methods Appl Fluoresc 2016;4:042005. https://doi.org/f9j8qj.
[42] Islam SDM, Susdorf T, Penzkofer A, Hegemann P. Fluorescence quenching of flavin adenine dinucleotide in aqueous solution by pH dependent isomerisation and photo-induced electron transfer. Chem Phys 2003;295:137–49. https://doi.org/d6k749.
[43] Grampp G, Hore PJ, Justinek M, Landgraf S, Lukzen NN. MARY spectroscopy: magnetic field effects on fluorescence intensities used for measuring electron transfer rates. Res Chem Intermed 2005;31:567–73. https://doi.org/c69mbv.
[44] Tarasov VV, Zoriniants GE, Shushin AI, Triebel MM. The role of spin-lattice relaxation in magnetic field effects on the luminescence of amorphous and polycrystalline rubrene films. Chem Phys Lett 1997;267:58–64. https://doi.org/c69mbv.
[45] Lewis AM, Fay TP, Manolopoulos DE, Kerpal C, Richert S, Timmel CR. On the low magnetic field effect in radical pair reactions. J Chem Phys 2018;149:034103. https://doi.org/gdxks2.
[46] Zadeh-Haghighi H, Simon C. Radical pairs can explain magnetic field and lithium effects on the circadian clock. Sci Rep 2022;12:269. https://doi.org/nkrw.
[47] Rishabh R, Zadeh-Haghighi H, Salahub D, Simon C. Radical pairs may explain reactive oxygen species-mediated effects of hypomagnetic field on neurogenesis. PLoS Comput Biol 2022;18. https://doi.org/nkrx.
[48] Van Huizen AV, Morton JM, Kinsey LJ, Von Kannon Donald G, Saad MA, Birkholz TR, et al. Weak magnetic fields alter stem cell-mediated growth. Sci Adv 2019;5. https://doi.org/gppq6d.